Check for updates

Advanced Electronic Materials

ADVANCED ELECTRONIC MATERIALS Open Access

www.advelectronicmat.de

RESEARCH ARTICLE OPEN ACCESS

Improved Hole Transport Layer Surface by Carbazole Ammonium Treatment for 988 nm Near-Infrared Tin-Lead Perovskite LEDs

Jiale Chen[1] | Jiaxiong Li[1] | David Garcia Romero[1] | Lijun Chen[1] | Han Wang[1] | Jane Kardula[2] | Ryan Chiechi[2,3] | Mordechai Kot[1] | Wouter T. M. Van Gompel[4,5,6] | Maria Antonietta Loi[1]

[1]Zernike Institute for Advanced Materials, University of Groningen, Groningen, The Netherlands | [2]Stratingh Institute for Chemistry, University of Groningen, Groningen, The Netherlands | [3]Department of Chemistry & Organic and Carbon Electronics Cluster, North Carolina State University, Raleigh, North Carolina, USA | [4]imec, imo-imomec, Diepenbeek, Belgium | [5]Institute for Materials Research (imo-imomec), Hybrid Materials Design (HyMaD), Hasselt University, Hasselt, Belgium | [6]Energyville, imo-imomec, Genk, Belgium

Correspondence: Maria Antonietta Loi (M.A.Loi@rug.nl)

Received: 23 June 2026 | **Revised:** 24 August 2026 | **Accepted:** 25 August 2026

Keywords: carrier lifetime | interface engineering | light-emitting diodes | near-infrared | tin-lead perovskite

ABSTRACT

Incorporating tin (Sn) and lead (Pb) into metal halide perovskites is an effective strategy for reducing bandgap energy, enabling applications in the near-infrared (NIR) spectral region. Recently, we demonstrated light-emitting diodes (LEDs) with long-wavelength emission peaks exceeding 900 nm. However, non-radiative recombination at the perovskite/transport layer interface remains a key limitation to device efficiency. In this work, we introduce carbazole ammonium iodide as an interfacial modifier, forming a hydrophilic thin layer atop the PEDOT:PSS hole transport layer. This interlayer enhances surface wettability, promotes improved perovskite crystallization, and facilitates better interface contact. The resulting perovskite films exhibit extended carrier lifetimes, and the corresponding NIR LEDs show reduced leakage current densities. Additionally, we systematically investigate the influence of annealing temperature on Sn–Pb-based perovskite film formation. X-ray diffraction (XRD) analysis reveals that high-temperature annealing accelerates crystallization but promotes PbI_2 formation, leading to rougher surfaces and increased crystal defects. By combining surface modification of the hole transport layer with optimized annealing conditions, we achieve a significant performance enhancement. The NIR LED with an emission peak at 988 nm exhibits a twofold increase in external quantum efficiency (EQE), improving from 0.6% to 1.3%, compared to devices using unmodified PEDOT:PSS.

1 | Introduction

Near-infrared (NIR) light-emitting diodes (LEDs) with emission wavelengths from 800 to 1000 nm have diverse applications, including night-vision devices, biomedical imaging, sensing and optical communications [1–3]. When looking for optoelectronic materials that are either low-cost, or easy to process, the availability of systems in the NIR decreases largely. Among solution-processable materials, organic semiconductors only recently made it to this spectral range [4, 5] and colloidal quantum dots have been shown to reach about 18% EQE with PbS [6, 7].

Metal halide perovskites have garnered significant attention for LED fabrication due to their narrow emission, tunable bandgaps, and high carrier mobility. Impressive efficiencies for perovskite light-emitting diodes (PeLEDs) have been reached in the visible range (32.14%, 32.1%, and 26.4% for red, green, and blue light, respectively [8–10]). Significant progress has been made also at

This is an open access article under the terms of the Creative Commons Attribution License, which permits use, distribution and reproduction in any medium, provided the original work is properly cited.
© 2026 The Author(s). *Advanced Electronic Materials* published by Wiley-VCH GmbH

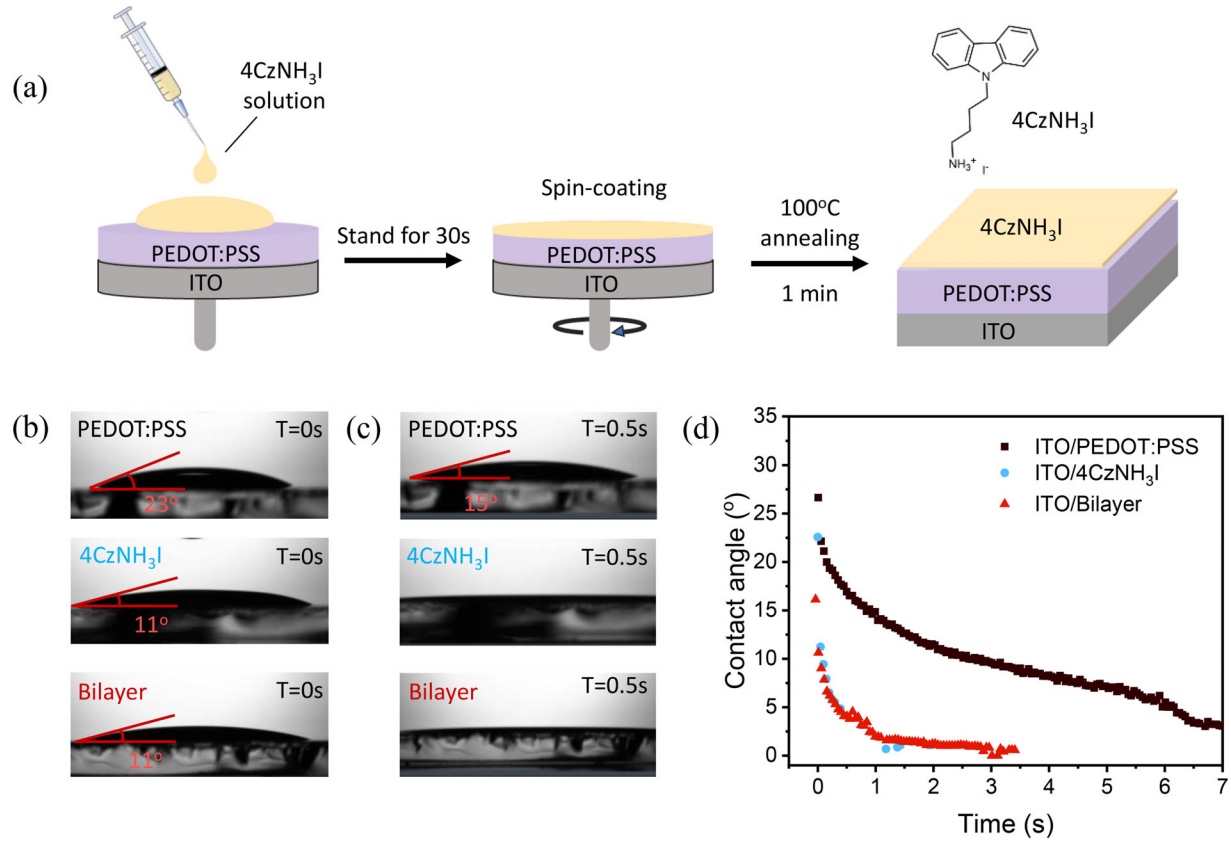


FIGURE 1 | (a) Fabrication procedure of $4CzNH_3I$ layer on top of PEDOT. (b) and (c): Contact angle images of drops of deionized water on films of PEDOT:PSS, $4CzNH_3I$, and bilayer at 0 s (b) and at 0.5 s (c), respectively. (d) Contact angle time evolution for different films.

the edge of the NIR where external quantum efficiencies (EQE) over 20% in the wavelength range between 700 and 900 nm [11, 12] have been reported. However, efficient NIR PeLEDs with an emission peak over 900 nm are still rare [13–15]. This challenge arises not only from the limited availability of materials that emit at such long wavelengths, but also from the increased susceptibility of near-infrared (NIR) emitters to non-radiative recombination. As the emission wavelength increases, non-radiative pathways become more competitive with radiative recombination, thereby limiting the performance of these materials in optoelectronic applications [5, 11, 16].

To date, all the NIR PeLEDs with emission peaks over 900 nm are prepared by tin (Sn)-based or Sn—Pb-based perovskite [2, 11, 13, 15]. Even though the alloying of Sn and Pb is the only strategy reported till now to reach a narrow bandgap in this class of materials, the introduction of tin poses challenges toward the demonstration of high-performance devices, such as the easy oxidation of Sn^{2+} to Sn^{4+}, the fast crystallization leading to non-optimal crystal quality, and the serious non-radiative recombination resulting from defective interfaces [17]. In the past, research efforts mainly focused on the suppression of the facile oxidation of Sn^{2+}, but less attention was given to the latter two [17–19]. In practice, fast crystallization of Sn-perovskite easily results in a poor crystal quality and high surface roughness, leading to serious leakage problems in devices [20, 21]. Furthermore, the energy loss from the non-radiative recombination at the interface can significantly affect not only the efficiency but also the stability of devices [22–24].

Poly(3,4-ethylenedioxythiophene):poly(styrenesulfonate) (PEDOT:PSS) is the most popular hole transport layer (HTL) material for tin or tin-lead based NIR PeLEDs, and there are not yet successful attempts to use the n-i-p structure, for either LEDs or solar cells with this family of active materials [14, 25–30]. PEDOT:PSS stands out from its good processability, high charge carrier mobility and excellent electron-blocking properties. However, PEDOT:PSS is often reported to be poorly compatible with metal halide perovskites. Its hygroscopic nature and acidity have been discussed as detrimental, together with the instability of its work function in contact with perovskites [31–33]. Furthermore, considering that the perovskite thin films are grown on top of the HTL, the properties of the latter, especially the surface energy and chemical composition, are of fundamental importance to the perovskite nucleation and the crystal growth [34]. Several authors have proposed to improve the performance of tin-based perovskite devices by adjusting the properties of the PEDOT:PSS-based HTL with additional layers [35–38].

Recently, we have reported a strategy for tuning the surface of a HTL from nonpolar to polar by depositing a carbazole alkylammonium iodide derivative ($4CzNH_3I$) on top of (2-(3,6-Dibromo-9H-carbazol-9-yl)ethyl)phosphonic acid (Br-2PACz) [39]. This strategy improved the wettability of Br-2PACz, reducing the defects at the interface between Sn/Pb perovskite films and the HTL. Building on this work, in this study a very low concentration $4CzNH_3I$ solution is deposited on top of the PEDOT:PSS to modify its surface chemistry. Contact angle measurements show that the wettability of PEDOT: PSS is improved after

2199160x, 2026, 20, Downloaded from https://advanced.onlinelibrary.wiley.com/doi/10.1002/aelm.70566, Wiley Online Library on [10/11/2026]. See the Terms and Conditions (https://onlinelibrary.wiley.com/terms-and-conditions) on Wiley Online Library for rules of use; OA articles are governed by the applicable Creative Commons License

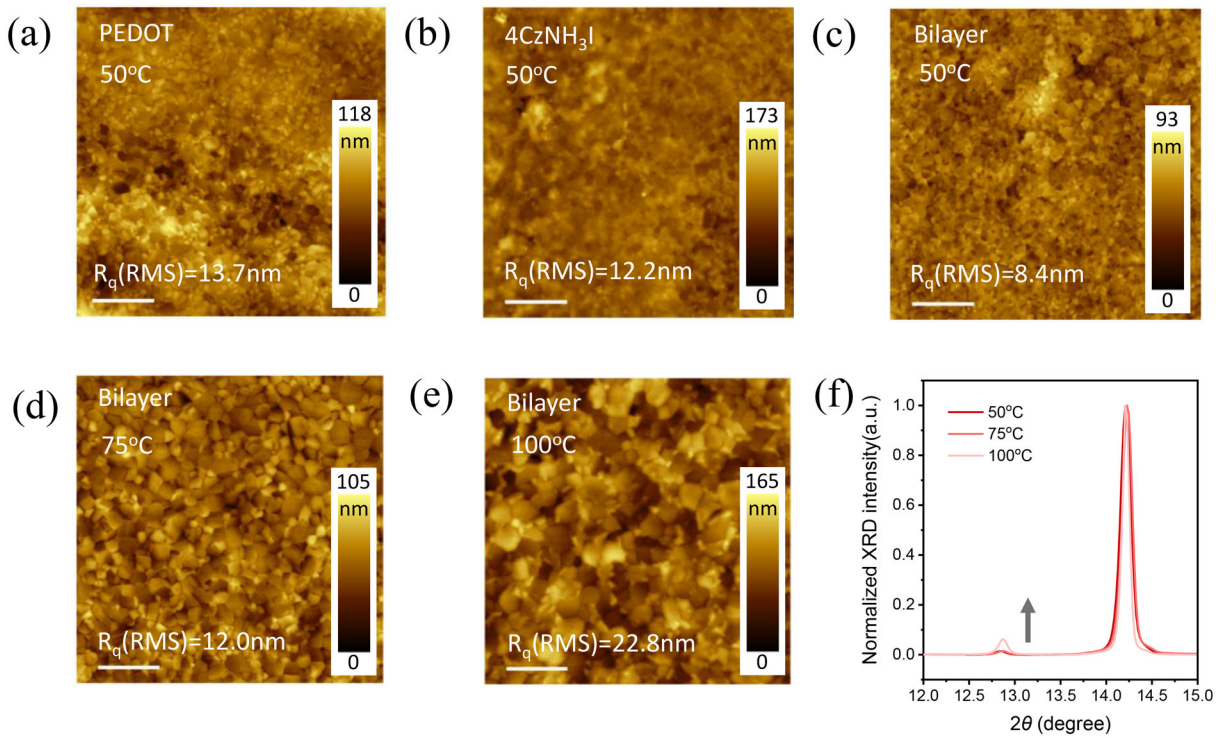


FIGURE 2 | AFM images of perovskite films on different HTLs: PEDOT (a), 4CzNH$_3$I (b), and bilayer (c), all annealed at 50°C. AFM images of perovskite films on bilayer with different annealing temperatures: 75°C (d) and 100°C (e). (f) XRD patterns of a $FA_{0.5}MA_{0.5}Sn_{0.5}Pb_{0.5}I_3$ perovskite film fabricated with different annealing temperature.

this step, with the surface becoming more polar. Atomic Force Microscopy (AFM) morphological investigation of the spin coated perovskite ($FA_{0.5}MA_{0.5}Sn_{0.5}Pb_{0.5}I_3$) films show that this bilayer strategy results in perovskite films with a smoother surface. Furthermore, we investigate the influence of different annealing temperatures on the crystallization of Sn/Pb-based perovskites. Perovskite films spin-coated on the PEDOT:PSS/4CzNH$_3$I and annealed at low-temperature show a smoother surface. XRD measurements show that samples annealed at high-temperature (100°C) contain a larger amount of lead-iodide impurities than the ones annealed at lower temperature (50°C). We found that the optimized film shows the longest carrier lifetime (216 ns) and the lowest leakage current in diode, indicating a reduce trap density. The results highlight the importance of synergistic control of the crystallization rate and interface engineering for high-quality Sn/Pb perovskite film. As a result, the optimized NIR PeLED show an EQE of 1.3% with the emission peak at 988 nm.

2 | Results and Discussion

Figure 1a shows the process utilized for depositing the 4CzNH$_3$I solution on top of PEDOT:PSS, namely by spin coating 1 mg/mL ethanol solution of 4CzNH$_3$I at 3000 rpm. Contact angle measurements were performed to examine the surface of the modified HTL. As shown in Figure 1b, a drop of deionized (DI) water on the pristine PEDOT:PSS film exhibited a contact angle of 23° at t = 0 s. As a comparison, for 4CzNH$_3$I alone on ITO, the corresponding contact angle is 11° at t = 0 s. The contact angle from the bilayer (PEDOT:PSS with 4CzNH$_3$I on top)-treated substrate also shows the similar number (11°) at t = 0 s, which indicate that 4CzNH$_3$I successfully modifies the PEDOT:PSS surface. Figure 1c clearly shows that the contact angle for a drop of DI water becomes too small to measure for the bilayer-treated film from time = 0.5 s while the contact angle on pristine PEDOT:PSS is still 15°. Figure 1d and Figure S1 visualize the variation of the contact angle with time utilizing the perovskite solution as probe. These experiments confirm that the wettability of PEDOT:PSS is significantly improved after depositing 4CzNH$_3$I. This is mainly attributed to its ammonium iodide moiety, which increases the hydrophilicity of the surface.

We then deposit perovskite films on the new improved HTL using a standard spin coating technique. The Sn/Pb perovskite solution was prepared as in our previous work [40]. 2,3,4,5,6-pentafluorophenethylammonium (5FPEA) (2.5 mol%) was added into the solution to passivate defects at the perovskite grain boundaries. Experimental details are described in the supporting information (SI). To investigate the effect of wettability on the film formation, Sn/Pb perovskite samples (annealed at 50°C) deposited on the different HTLs (PEDOT, 4CzNH$_3$I, and bilayer) were prepared. In addition, we also prepared bilayer samples with different annealing temperatures to investigate the effect of the crystallization rate on the Sn/Pb perovskite.

From AFM measurements (Figure 2a–c), a lower perovskite film roughness when the active layer is deposited on the bilayer sample is found (Rq = 8.4 nm compared to Rq = 13.7 nm from PEDOT-based sample). This smooth morphology indicates that the crystallization is more uniform giving rise to a more compact and higher quality film, which is likely due to the improvement of interface wettability. Figure S2 shows the X-ray diffraction (XRD)

2199160x, 2026, 20, Downloaded from https://advanced.onlinelibrary.wiley.com/doi/10.1002/aelm.70566, Wiley Online Library on [10/11/2026]. See the Terms and Conditions (https://onlinelibrary.wiley.com/terms-and-conditions) on Wiley Online Library for rules of use; OA articles are governed by the applicable Creative Commons License

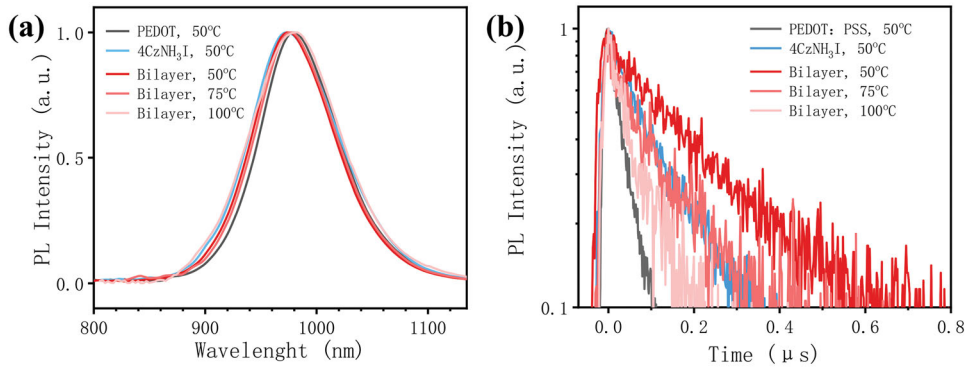


FIGURE 3 | (a) Normalized PL spectra and (b) TRPL decays of $FA_{0.5}MA_{0.5}Sn_{0.5}Pb_{0.5}I_3$ films on different HTLs and different annealing temperatures.

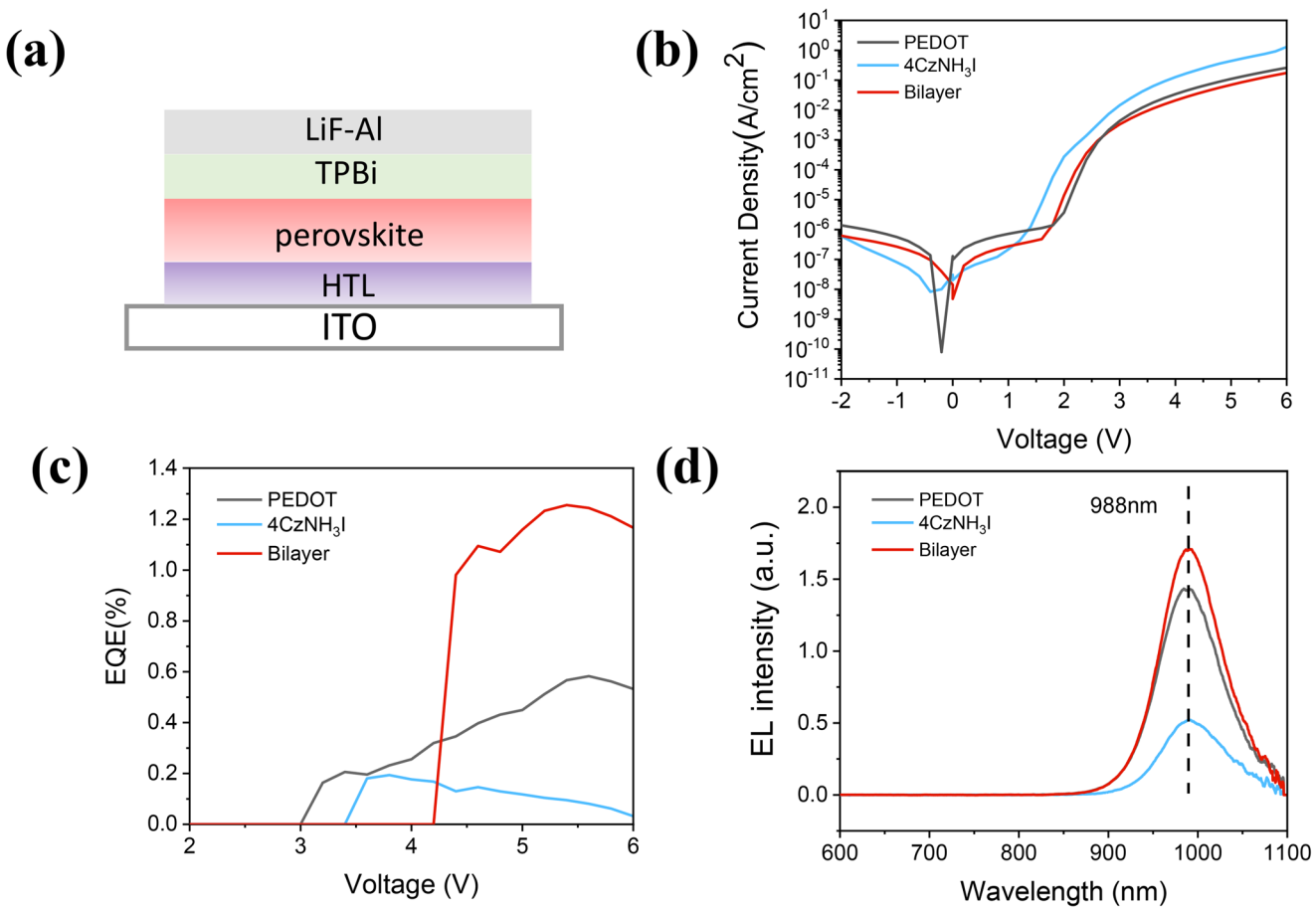


FIGURE 4 | NIR LED performance of PEDOT:PSS, $4CzNH_3I$, and bilayer-based perovskite devices. (a) Device structure. (b) Typical urrent density-voltage (J-V) curves for devices using different HTLs. (c) EQE-voltage curves and (d) EL spectra of NIR PeLEDs.

patterns for samples deposited on different HTLs, similar peak locations and intensities can be observed.

Furthermore, we found that the annealing temperature has a great influence on the perovskite morphology and crystallinity. We focus for this experiment on the bilayer HTL, in the AFM micrograph (Figure 2d,e) the fast crystallization resulted in a larger grain size and a rougher surface as the perovskite annealing temperature was increased from 50°C to 100°C. From the XRD pattern in Figure S2a, the diffraction peak at 14.2° corresponding to (100) perovskite planes increases in intensity with increasing annealing temperature. However, with the increase of the annealing temperature, the signal of lead iodide (PbI_2) at 12.7° also becomes more prominent, both in Figure S2b for its absolute intensity, and in Figure 2f when the data is normalized at the 14.2° perovskite peak. Therefore, the high temperature annealing seems to cause the formation of PbI_2 impurities, which are detrimental for device performance and stability.

2199160x, 2026, 20, Downloaded from https://advanced.onlinelibrary.wiley.com/doi/10.1002/aelm.70566, Wiley Online Library on [10/11/2026]. See the Terms and Conditions (https://onlinelibrary.wiley.com/terms-and-conditions) on Wiley Online Library for rules of use; OA articles are governed by the applicable Creative Commons License

Next, we performed steady-state and time-resolved photoluminescence (PL) measurements to investigate the optical properties and the carrier recombination dynamics of the perovskite films grown on different substrates. As shown in Figure 3a, all the films show a similar single emission peak at around 990 nm with a full width at half maximum (FWHM) of around 90 nm. In the time-resolved photoluminescence (TRPL) measurement, the perovskite film grown on PEDOT-PSS shows a carrier lifetime of 38 ns while that of the film grown on $4CzNH_3I$ is 108 ns. With the surface-modified PEDOT:PSS, the carrier lifetime of the perovskite active layer (50°C annealing) drastically increased to 216 ns. This significantly extended carrier lifetime can be attributed to the improved perovskite-HTL interface and the passivation effects of the ammonium iodide group in $4CzNH_3I$ on the perovskite buried interface, resulting in reduced nonradiative recombination [41, 42]. By studying the annealing temperature effects, we also observe that the carrier lifetime decreases from 216 to 112 ns and 81 ns as the temperature increased from 50°C to 75°C and 100°C, respectively. Based on the investigation of XRD measurement, we believe that excessive lead iodide generates a large number of trapping states, which leads to a reduction of the carrier lifetime.

We fabricate the Sn/Pb based NIR PeLEDs with the following device architecture (Figure 4a): indium tin oxide (ITO)/HTL/perovskite active layer/TPBi (35 nm)/LiF (1 nm)/Al (100 nm). Figure 4b shows the J-V characteristics of the devices with different HTLs. Here we can observe that both devices employing $4CzNH_3I$ as HTL show a lower leakage current than the device made from PEDOT:PSS only. Based on what we observed in the morphological investigation, we believe that this low leakage can mainly be attributed to the improved interface contacts of the $4CzNH_3I$ containing samples. The external quantum efficiency (EQE) curves measured from different devices are summarized in Figure 4c. The devices using the bilayer as HTL shows the highest EQE of 1.3% and achieves a maximum irradiance of 22 $W/sr/m^2$ (Figure S3). Table S1 summarize the EQE values and emission wavelengths of representative Sn-based and Sn/Pb-based NIR perovskite LEDs reported in the literature, together with our device. All devices showed the same electroluminescence peaks at 988 nm (Figure 4d), with the bilayer device showing the highest EL intensity. The reason why the electroluminescence of the PEDOT-based devices is higher than that of the devices fabricated from $4CzNH_3I$ on ITO is possibly related to the electron blocking capabilities of PEDOT:PSS that encourages radiative recombination in the active material, which makes employing PEDOT:PSS in the layer stack still attractive. However, also the difference in orientation of the $4CzNH_3I$ molecules on ITO and on PEDOT:PSS may have an influence on the optoelectronic properties of LEDs as well as on the roughness and morphology of the perovskite film (see Figure 2b,c).

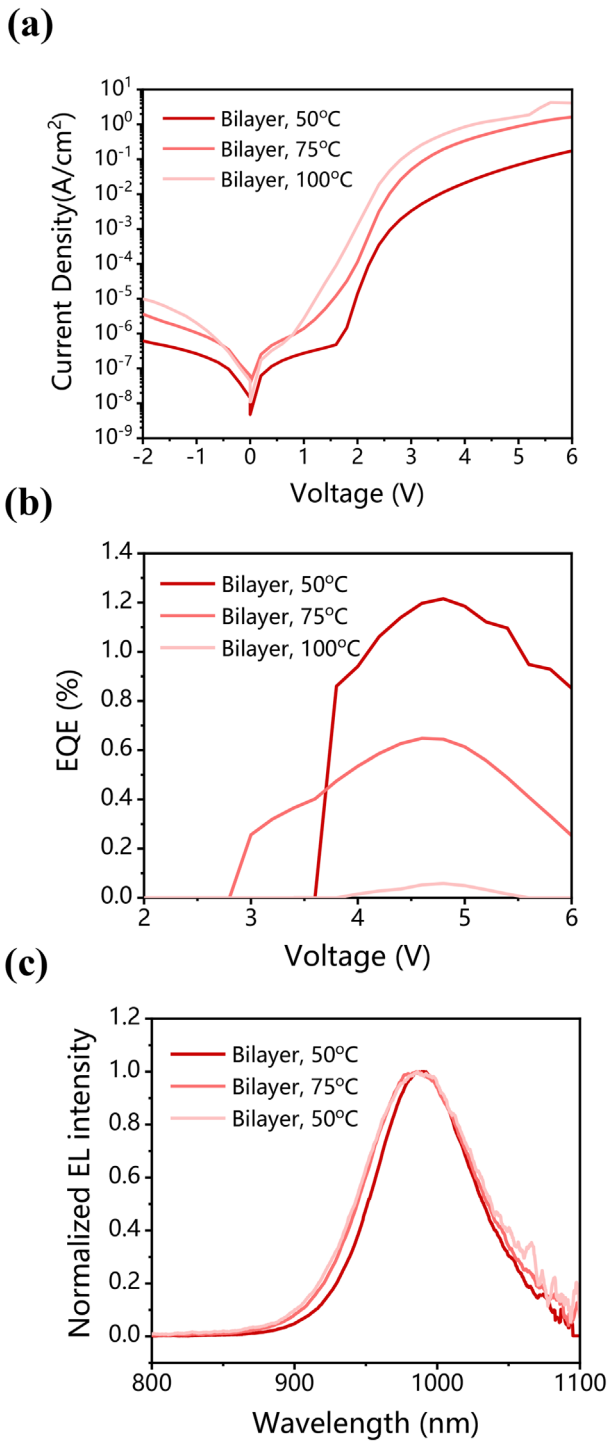


FIGURE 5 | (a) Current density-voltage curves, (b) EQE-voltage curves and (c) normalized EL spectral of the infrared PeLED fabricated utilising different annealing temperature.

To obtain further insights on carrier transport, impedance measurements were performed. Figure S4 shows the measured capacitance versus frequency in these devices. Although PEDOT:PSS and PEDOT:PSS/$4CzNH_3I$ show similar low-frequency capacitance, indicating comparable charge accumulation at long timescales, which might also include ion migration contributions, their frequency response is markedly different. The PEDOT:PSS-based sample exhibits a sharp capacitance drop around 1 kHz, suggesting the presence of interfacial states or mobile charges (protons) given their characteristic response times in the microsecond range. In contrast, when $4CzNH_3I$ is added on top of PEDOT:PSS, a nearly constant capacitance until much higher frequencies is reached, directly pointing to a more inert material system. This is in line with previous reports where a highly resistive or dielectric HTL limits dynamic charge exchange across the interface [43, 44]. This could also explain the delay in

2199160x, 2026, 20, Downloaded from https://advanced.onlinelibrary.wiley.com/doi/10.1002/aelm.70566, Wiley Online Library on [10/11/2026]. See the Terms and Conditions (https://onlinelibrary.wiley.com/terms-and-conditions) on Wiley Online Library for rules of use; OA articles are governed by the applicable Creative Commons License

EQE switch-on of the bilayer LED device as seen in Figure 4c, along with its low leakage characteristics.

Overall, by leveraging the electron blocking mechanisms (benefited from the high LUMO of PEDOT) and the improved interface for favorable perovskite crystallization and charge injection (assisted by the $4CzNH_3I$ surface treatment), we can achieve superior NIR LED performance.

Finally, we compare the NIR LEDs fabricated with Sn/Pb perovskite films annealed at 50°C, 75°C, and 100°C. As shown in Figure 5a, the device annealed at 50°C shows the lowest leakage current and the highest EQE (Figure 5b), in accordance with its better surface morphology and phase purity. Both the leakage current and the FWHM of the EL signal (Figure 5c) increase as the annealing temperature increases (83, 90, and 93 nm for 50°C, 75°C, and 100°C, respectively), showing that a proper annealing temperature control is critical in preserving good Sn/Pb perovskite crystal quality and LED performance.

3 | Conclusions

In this study, we engineer the wettability of the prototypical PEDOT:PSS HTL layer via the deposition of $4CzNH_3I$ molecules. The perovskite thin film shows a more uniform and smoother morphology using this strategy, which also incurs lower interface losses. The XRD and AFM investigations further show that low-temperature perovskite annealing is critical for avoiding the formation of PbI_2 and for obtaining a smooth film morphology. TRPL measurements confirms that the optimized perovskite film possesses a longer carrier lifetime, which is essential for the good functioning of the LED. The NIR LEDs employing bilayer HTL, and annealed at 50°C shows reduced leakage current, increased EL intensity, resulting in an EQE of 1.3% at 988 nm emission.

Acknowledgements

The authors would like to express their gratitude for the technical assistance from Arjen Kamp and Teodor Zaharia. Jiale Chen appreciates financial funding from the Chinese Scholar Council (CSC). This work is funded by the European Union (ERC-AdvancedGrant, DEOM, 101055097). Views and opinions expressed are however, those of the author(s) only and do not necessarily reflect those of the European Union or the European Research Council. Neither the European Union nor the granting authority can be held responsible for them.

Conflicts of Interest

The authors declare no conflicts of interest.

Data Availability Statement

The data that support the findings of this study are openly available in DataverseNL at https://doi.org/10.34894/VVI9RJ.

References

1. W.-L. Hong, Y.-C. Huang, and C.-Y. Chang, "Efficient Low-Temperature Solution-Processed Lead-Free Perovskite Infrared Light-Emitting Diodes," *Advanced Materials* 28, no. 36 (2016): 8029–8036.

2. W. Qiu, Z. Xiao, and K. Roh, "Mixed Lead–Tin Halide Perovskites for Efficient and Wavelength-Tunable Near-Infrared Light-Emitting Diodes," *Advanced Materials* 31, no. 3 (2019): 1806105.

3. M. Vasilopoulou, A. Fakharuddin, and F. P. García de Arquer, "Advances in Solution-Processed Near-Infrared Light-Emitting Diodes," *Nature Photonics* 15, no. 9 (2021): 656–669, https://doi.org/10.1038/s41566-021-00855-2.

4. S. Ahadzadeh, S. Brebels, W. Maes, and W. Deferme, "Strategies for Advancing Near-Infrared Organic Light-Emitting Diodes: Innovations in Luminescent Materials, Device Architectures, Fabrication Methods, and Applications," *Advanced Functional Materials* 36 (2025): 2419599.

5. P. L. dos Santos, P. Stachelek, Y. Takeda, and P. Pander, "Recent Advances in Highly-Efficient Near Infrared OLED Emitters," *Materials Chemistry Frontiers* 8, no. 7 (2024): 1731–1766, https://doi.org/10.1039/D3QM01067H.

6. A. G. Shulga, S. Kahmann, and D. N. Dirin, "Electroluminescence Generation in PbS Quantum Dot Light-Emitting Field-Effect Transistors With Solid-State Gating," *ACS Nano* 12, no. 12 (2018): 12805–12813, https://doi.org/10.1021/acsnano.8b07938.

7. S. Pradhan, M. Dalmases, N. Taghipour, B. Kundu, and G. Konstantatos, "Colloidal Quantum Dot Light Emitting Diodes at Telecom Wavelength With 18% Quantum Efficiency and over 1 MHz Bandwidth," *Advanced Science* 9, no. 20 (2022): 2200637.

8. S.-Q. Sun, J.-W. Tai, W. He, et al., "Enhancing Light Outcoupling Efficiency via Anisotropic Low Refractive Index Electron Transporting Materials for Efficient Perovskite Light-Emitting Diodes," *Advanced Materials* 36, no. 24 (2024): 2400421.

9. Y. Gao, Q. Cai, and Y. He, "Highly Efficient Blue Light-emitting Diodes Based on Mixed-halide Perovskites With Reduced Chlorine Defects," *Science Advances* 10, no. 29 (2024): ado5645, https://doi.org/10.1126/sciadv.ado5645.

10. S.-C. Feng, Y. Shen, and X.-M. Hu, "Efficient and Stable Red Perovskite Light-Emitting Diodes via Thermodynamic Crystallization Control," *Advanced Materials* 36, no. 44 (2024): 2410255.

11. Y. Liu, F. Di Stasio, C. Bi, et al., "Near-Infrared Light Emitting Metal Halides: Materials, Mechanisms, and Applications," *Advanced Materials* 36, no. 21 (2024): 2312482, https://doi.org/10.1002/adma.202312482.

12. Y. Sun, L. Ge, and L. Dai, "Bright and Stable Perovskite Light-Emitting Diodes in the Near-Infrared Range," *Nature* 615, no. 7954 (2023): 830–835, https://doi.org/10.1038/s41586-023-05792-4.

13. F. Yuan, G. Folpini, and T. Liu, "Bright and Stable Near-Infrared Lead-Free Perovskite Light-Emitting Diodes," *Nature Photonics* 18, no. 2 (2024): 170–176, https://doi.org/10.1038/s41566-023-01351-5.

14. J. Lu, X. Guan, and Y. Li, "Dendritic $CsSnI_3$ for Efficient and Flexible Near-Infrared Perovskite Light-Emitting Diodes," *Advanced Materials* 33, no. 44 (2021): 2104414.

15. H. Yu, W. Chen, Z. Fang, L. Ding, B. Cao, and Z. Xiao, "Alkalis-Doping of Mixed Tin-Lead Perovskites for Efficient Near-Infrared Light-Emitting Diodes," *Science Bulletin* 67, no. 1 (2022): 54–60.

16. C.-M. Hung, S.-F. Wang, and W.-C. Chao, "High-Performance Near-Infrared OLEDs Maximized at 925 and 1022 Nm Through Interfacial Energy Transfer," *Nature Communications* 15, no. 1 (2024): 4664, https://doi.org/10.1038/s41467-024-49127-x.

17. W.-F. Yang, F. Igbari, Y.-H. Lou, Z.-K. Wang, and L.-S. Liao, "Tin Halide Perovskites: Progress and Challenges," *Advanced Energy Materials* 10, no. 13 (2020): 1902584.

18. J. Cao, H.-L. Loi, and Y. Xu, "High-Performance Tin–Lead Mixed-Perovskite Solar Cells With Vertical Compositional Gradient," *Advanced Materials* 34, no. 6 (2022): 2107729, https://doi.org/10.1002/adma.202107729.

19. B. Li, B. Chang, and L. Pan, "Tin-Based Defects and Passivation Strategies in Tin-Related Perovskite Solar Cells," *ACS Energy Letters* 5, no. 12 (2020): 3752–3772, https://doi.org/10.1021/acsenergylett.0c01796.

2199160x, 2026, 20, Downloaded from https://advanced.onlinelibrary.wiley.com/doi/10.1002/aelm.70566, Wiley Online Library on [10/11/2026]. See the Terms and Conditions (https://onlinelibrary.wiley.com/terms-and-conditions) on Wiley Online Library for rules of use; OA articles are governed by the applicable Creative Commons License

20. J. Wang, K. Datta, J. Li, et al., "Understanding the Film Formation Kinetics of Sequential Deposited Narrow-Bandgap Pb–Sn Hybrid Perovskite Films," *Advanced Energy Materials* 10, no. 22 (2020): 2000566.

21. M. Konstantakou and T. Stergiopoulos, "A Critical Review on Tin Halide Perovskite Solar Cells," *Journal of Materials Chemistry A* 5, no. 23 (2017): 11518–11549, https://doi.org/10.1039/C7TA00929A.

22. Y. Zou, T. Wu, and F. Fu, "Thermal-Induced Interface Degradation in Perovskite Light-Emitting Diodes," *Journal of Materials Chemistry C* 8, no. 43 (2020): 15079–15085, https://doi.org/10.1039/D0TC03816D.

23. Y.-C. Ye, Y.-Q. Li, and X.-Y. Cai, "Minimizing Optical Energy Losses for Long-Lifetime Perovskite Light-Emitting Diodes," *Advanced Functional Materials* 31, no. 46 (2021): 2105813.

24. L. Zhao, K. M. Lee, K. Roh, S. U. Z. Khan, and B. P. Rand, "Improved Outcoupling Efficiency and Stability of Perovskite Light-Emitting Diodes Using Thin Emitting Layers," *Advanced Materials* 31, no. 2 (2019): 1805836.

25. Y. Meng, X. Guan, and Y. Weng, "Bi-Functional Phosphine Oxide Passivator for Efficient Near-Infrared Sn-Based Perovskite Light-Emitting Diodes With Ultra-Low Efficiency Roll-Off," *Advanced Functional Materials* 34, no. 13 (2024): 2310530.

26. Y. Shen, Z. Tang, J. Chen, T. Zhang, L. Qian, and C. Xiang, "The Improvement of Tin-Based Perovskite Thin Film Quality to Enhance the Performance of Near-Infrared PeLEDs Through Thiocyanate Modification," *Advanced Optical Materials* 12, no. 20 (2024): 2400398.

27. F. Zhang, H. Min, Y. Zhang, et al., "Vapor-Assisted in Situ Recrystallization for Efficient Tin-Based Perovskite Light-Emitting Diodes," *Advanced Materials* 34, no. 37 (2022): 2203180.

28. M. L. Lai, T. Y. S. Tay, and A. Sadhanala, "Tunable Near-Infrared Luminescence in Tin Halide Perovskite Devices," *The Journal of Physical Chemistry Letters* 7, no. 14 (2016): 2653–2658, https://doi.org/10.1021/acs.jpclett.6b01047.

29. X.-Z. Li, Y. Ye, Y. Cao, et al., "Tin-Halide Perovskites for Light-Emitting Diodes," *Chemical Society Reviews* 54 (2025): 6697–6725, https://doi.org/10.1039/D5CS00340G.

30. W. Ke, C. Chen, and I. Spanopoulos, "Narrow-Bandgap Mixed Lead/Tin-Based 2D Dion–Jacobson Perovskites Boost the Performance of Solar Cells," *Journal of the American Chemical Society* 142, no. 35 (2020): 15049–15057, https://doi.org/10.1021/jacs.0c06288.

31. F. M. Rombach, A. Dasgupta, and M. Kober-Czerny, "Disentangling Degradation Pathways of Narrow Bandgap Lead-Tin Perovskite Material and Photovoltaic Devices," *Nature Communications* 16, no. 1 (2025): 5450, https://doi.org/10.1038/s41467-025-58489-9.

32. B. J. Bruijnaers, E. Schiepers, C. H. L. Weijtens, S. C. J. Meskers, M. M. Wienk, and R. A. J. Janssen, "The Effect of Oxygen on the Efficiency of Planar p–i–n Metal Halide Perovskite Solar Cells With a PEDOT:PSS Hole Transport Layer," *Journal of Materials Chemistry A* 6, no. 16 (2018): 6882–6890, https://doi.org/10.1039/C7TA11128B.

33. R. Prasanna, T. Leijtens, and S. P. Dunfield, "Design of Low Bandgap Tin–Lead Halide Perovskite Solar Cells to Achieve Thermal, Atmospheric and Operational Stability," *Nature Energy* 4, no. 11 (2019): 939–947, https://doi.org/10.1038/s41560-019-0471-6.

34. Z. T. Gebremichael, C. Ugokwe, S. Alam, et al., "How Varying Surface Wettability of Different PEDOT:PSS Formulations and Their Mixtures Affects Perovskite Crystallization and the Efficiency of Inverted Perovskite Solar Cells," *RSC Advances* 12, no. 39 (2022): 25593–25604, https://doi.org/10.1039/D2RA03843A.

35. C. Bi, Q. Wang, Y. Shao, Y. Yuan, Z. Xiao, and J. Huang, "Non-Wetting Surface-Driven High-Aspect-Ratio Crystalline Grain Growth for Efficient Hybrid Perovskite Solar Cells," *Nature Communications* 6, no. 1 (2015): 7747, https://doi.org/10.1038/ncomms8747.

36. M. Degani, Q. An, and M. Albaladejo-Siguan, "23.7% Efficient Inverted Perovskite Solar Cells by Dual Interfacial Modification," *Science Advances* 7, no. 49 (2021): eabj7930, https://doi.org/10.1126/sciadv.abj7930.

37. C.-C. Shih and C.-G. Wu, "Synergistic Engineering of the Conductivity and Surface Properties of PEDOT:PSS-Based HTLs for Inverted Tin Perovskite Solar Cells to Achieve Efficiency Over 10%," *ACS Applied Materials & Interfaces* 14 (2022): 16125–16135, https://doi.org/10.1021/acsami.1c22262.

38. S. J. Yang, D. Varadharajan, and K. Tateno, "Interfacial Molecular Engineering for Efficient Sn Perovskite Light-Emitting Diodes," *ACS Photonics* 11 (2024): 4941–4947, https://doi.org/10.1021/acsphotonics.4c01467.

39. M. Pitaro, J. S. Alonso, and L. Di Mario, "A Carbazole-Based Self-Assembled Monolayer as the Hole Transport Layer for Efficient and Stable $Cs_{0.25}$ $FA_{0.75}$ $Sn_{0.5}$ $Pb_{0.5}$ I_3 Solar Cells," *Journal of Materials Chemistry A* 11 (2023): 11755–11766, https://doi.org/10.1039/D3TA01276J.

40. J. Chen, J. Li, R. Pau, et al., "1.4% External Quantum Efficiency 988 Nm Light Emitting Diode Based on Tin-Lead Halide Perovskite," *Advanced Materials* 37, no. 25 (2025): 2415958.

41. G. Yang, C. Wang, H. Lei, et al., "Interface Engineering in Planar Perovskite Solar Cells: Energy Level Alignment, Perovskite Morphology Control and High Performance Achievement," *Journal of Materials Chemistry A* 5, no. 4 (2017): 1658–1666, https://doi.org/10.1039/C6TA08783C.

42. M. Pitaro, J. E. S. Alonso, and L. Di Mario, "Tuning the Surface Energy of Hole Transport Layers Based on Carbazole Self-Assembled Monolayers for Highly Efficient Sn/Pb Perovskite Solar Cells," *Advanced Functional Materials* 34, no. 50 (2024): 2306571.

43. E. von Hauff and D. Klotz, "Impedance Spectroscopy for Perovskite Solar Cells: Characterisation, Analysis, and Diagnosis," *Journal of Materials Chemistry C* 10, no. 2 (2022): 742–761, https://doi.org/10.1039/D1TC04727B.

44. X. Qu and X. Sun, "Impedance Spectroscopy for Quantum Dot Light-Emitting Diodes," *Journal of Semiconductors* 44 (2023): 091603, https://doi.org/10.1088/1674-4926/44/9/091603.

Supporting Information

Additional supporting information can be found online in the Supporting Information section.

Supporting File: aelm70566-sup-0001-SuppMat.docx.

2199160x, 2026, 30, Downloaded from https://advanced.onlinelibrary.wiley.com/doi/10.1002/aelm.70566, Wiley Online Library on [10/11/2026]. See the Terms and Conditions (https://onlinelibrary.wiley.com/terms-and-conditions) on Wiley Online Library for rules of use; OA articles are governed by the applicable Creative Commons License